Surface Conductance Induced Dielectrophoresis of Semiconducting Single-Walled Carbon Nanotubes

ARTICLE *in* NANO LETTERS · AUGUST 2004

Impact Factor: 13.59 · DOI: 10.1021/nl0493794

4 AUTHORS, INCLUDING:

Ralph Krupke
Karlsruhe Institute of Technology
95 PUBLICATIONS **3,939** CITATIONS

SEE PROFILE

Frank Hennrich
Karlsruhe Institute of Technology
158 PUBLICATIONS **6,914** CITATIONS

SEE PROFILE

NANO LETTERS

2004
Vol. 4, No. 8
1395−1399

Surface Conductance Induced Dielectrophoresis of Semiconducting Single-Walled Carbon Nanotubes

Ralph Krupke,*,† Frank Hennrich,† Manfred M. Kappes,†,‡ and Hilbert v. Löhneysen§,||

Forschungszentrum Karlsruhe, Institut für Nanotechnologie, D-76021 Karlsruhe, Germany, Institut für Physikalische Chemie, Universität Karlsruhe, D-76128 Karlsruhe, Germany, Physikalisches Institut, Universität Karlsruhe, D-76128 Karlsruhe, Germany, Forschungszentrum Karlsruhe, Institut für Festkörperphysik, D-76021 Karlsruhe, Germany

Received April 28, 2004; Revised Manuscript Received June 3, 2004

ABSTRACT

Dielectrophoresis on surfactant-stabilized single-walled carbon nanotube (SWNT) suspensions has been demonstrated to separate metallic from semiconducting tubes by their different electric field-induced polarizabilities. Here we report that the interaction between SWNTs and the surfactant induces a nanotube surface conductance which gives rise to a unique electric field frequency dependence of the nanotube dielectrophoresis. We observe a surfactant concentration dependent crossover frequency enabling separation of metallic from semiconducting SWNTs at high frequency and deposition of metallic and semiconducting SWNTs at low frequency – both being important aspects for building nanotube-based electronics. Moreover, the data demonstrate that the theoretical description of dielectrophoretic forces is valid beyond the dimensions of cells or viruses.

Single-walled carbon nanotubes (SWNTs) have become promising building blocks for future nanoscale electronics due to their exceptional electronic and structural properties.[1] Although composed purely of carbon, SWNTs exist in metallic and semiconducting modifications because of quantum size effects. Both tube types, with variations in diameter and degree of chirality, are grown together, independent of the production method used.[2] This mixed appearance of tubes has been regarded as an obstacle for possible future electronic applications. Recently it has been demonstrated that metallic SWNTs can be separated from semiconducting SWNTs by their opposite movement in a solvent when interacting with an external alternating electric field.[3] The effect is based on the different electric-field induced polarizabilities of the two tube types. In this work we compare samples prepared via dielectrophoresis at various electric-field frequencies and solvent conductivities and reference samples and conclude that micellization of SWNTs induces a finite nanotube surface conductance, which gives rise to a frequency dependence of the nanotube dielectrophoresis.

For the experiments we prepared SWNT suspensions by sonicating 100 mL D_2O containing 0.05 weight % HiPco raw material (10 mg) and 1 weight % of the surfactant sodium dodecylbenzene sulfonate (SDBS), similar to the procedure described in ref 4. After sonication, the suspensions were centrifuged at 154000 g for 2 h and the upper 90% of the supernatant was carefully decanted. The suspensions thus obtained exhibit sharp features in the electronic absorption spectra and strong fluorescence, which is indicative of a high percentage of individually suspended SWNTs rather than bundles. Suspensions containing 0.1 weight % and 0.01 weight % SDBS were obtained by successively diluting with D_2O. The critical micelle concentration (CMC) for SDBS in water is 2.8 mmol/L or 0.097 weight %.[5] Hence, our suspensions with 0.01% SDBS, 0.1% SDBS, and 1% SDBS are well below, at, and well above the CMC, respectively. Microelectrodes with a gap of 10 μm were prepared by standard electron beam lithography and wired to a function generator (Figure 1), which was operated at a frequency f ranging from 30 kHz up to 30 MHz and a peak-to-peak voltage of (Vp-p) 20 V. Separate samples, each with 15 electrode pairs, have been prepared for each combination of frequency and surfactant concentration. After the generator was switched on, a drop of suspension ($\sim$10 μL) was applied onto the chip. After a delay of 10 min, the samples were rinsed with H_2O and the generator was switched off. Finally the samples were rinsed in ethanol and dried in a stream of nitrogen gas. Reference samples were prepared by putting a

* Corresponding author. E-mail: ralph.krupke@int.fzk.de.
† Forschungszentrum Karlsruhe, Institut für Nanotechnologie.
‡ Institut für Physikalische Chemie, Universität Karlsruhe.
§ Physikalisches Institut, Universität Karlsruhe.
|| Forschungszentrum Karlsruhe, Institut für Festkörperphysik.

10.1021/nl0493794 CCC: $27.50
Published on Web 07/13/2004

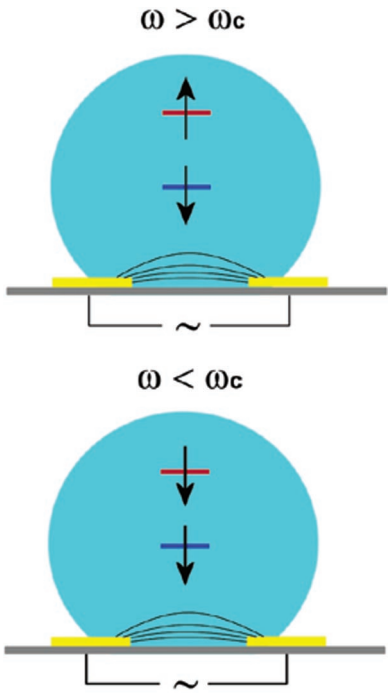

Figure 1. Schematic cross section of the experimental setup during dielectrophoresis showing microelectrodes wired to an ac generator. Gold electrodes (yellow) are 20 nm thick, 1 μm wide, and have a gap of 10 μm on a p-type silicon substrate with 600 nm of thermally oxidized SiO_2. A thin Ti adhesion layer was used. The lines illustrate the electric field during deposition when a drop of suspended SWNTs is applied to the surface (cyan). Metallic SWNTs (blue) and semiconducting SWNTs (red) interact with the ac field with positive dielectrophoresis (↓) or negative dielectrophoresis (↑) depending on the frequency ω. ω_c is the crossover frequency (see text).

drop of suspension for each surfactant concentration on a silicon substrate and letting it dry. The samples were characterized with a confocal Raman microscope excited with an Ar^+ ion laser at 514.5 nm excitation. The laser spot had a diameter of ~1 μm on the sample with a power density of $\sim 10^5$ W/cm^2. The Raman spectra were recorded with the polarization of the incident light in parallel to the long axis of the electrodes and a spectral resolution of 3.75 cm^{-1}. In addition, we characterized the samples with optical and scanning electron microscopy.

Figure 2 shows dark-field micrographs and scanning electron microscopy images of samples deposited via DEP from a 0.1% SDBS suspension at two different frequencies. The images show that the individually suspended tubes form bundles at surfaces once they are deposited onto the electrodes. Similar morphologies are observed for the other samples as well. The formation of bundles at the surface and the wide diameter distribution of the HiPco tube batch used (0.8 nm − 1.4 nm) allows to probe several metallic and semiconducting SWNTs with resonant Raman spectroscopy by using the single wavelength $\lambda = 514.5$ nm.[3,6]

Figure 3 shows Raman spectra of tubes deposited with eight different frequencies, each from suspensions with three different surfactant concentrations including the reference samples. The data were obtained by averaging the Raman spectra recorded at 10 different electrode pairs. We begin to analyze the composition of our deposited samples by studying the Raman signal of samples prepared from 0.01% SDBS suspensions (Figure 3a). As described in detail in ref 3, we distinguish in our experiment between metallic and semiconducting tubes by their corresponding radial breathing modes (RBM) and their tangential G-modes (G^+, G^-). The probed semiconducting SWNTs contribute to RBM modes around 180 cm^{-1} and to sharp G modes, with the G^+ mode being much stronger than the G^- mode. The probed metallic SWNTs contribute to RBM modes around 260 cm^{-1}, a broad G^-, mode and a small G^+ mode. The abundance of metallic and semiconducting SWNTs is reflected by the intensities of the corresponding Raman modes. For the 0.01% SDBS reference sample we observe Raman intensity in both RBM mode regions, a broad G^- mode and a strong and sharp G^+ mode. Such a spectrum is expected for the reference sample which contains metallic and semiconducting SWNTs in the same ratio as present in suspension. The spectra of 0.01% SDBS tubes deposited via DEP at different frequencies look very similar for both RBM and G mode intensities. Even for the 30 MHz sample semiconducting tubes are detected. Hence, for the 0.01% SDBS samples we do not observe a significant separation of metallic from semiconducting tubes

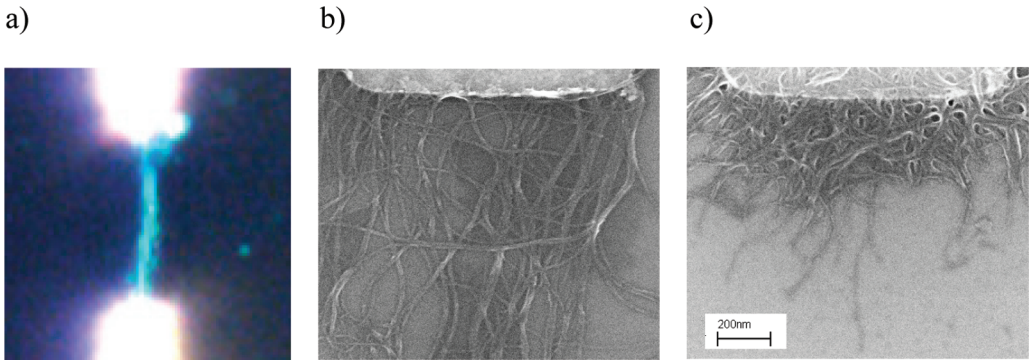

Figure 2. (a−c) Top-view images of a low- and high-frequency sample after dielectrophoretic deposition from a 0.1% SDBS suspension and after solvent removal. Incident-light dark-field microscopy image of SWNTs deposited at 3 MHz onto 10 μm gapped gold electrodes (a); scanning electron microscopy images of a sample deposited at 3 MHz (b) and at 300 kHz (c). Although SWNTs were suspended individually, they form bundles on the surface. Samples containing only metallic tubes form macroscopically elongated structures due to local electrical field enhancement during deposition.

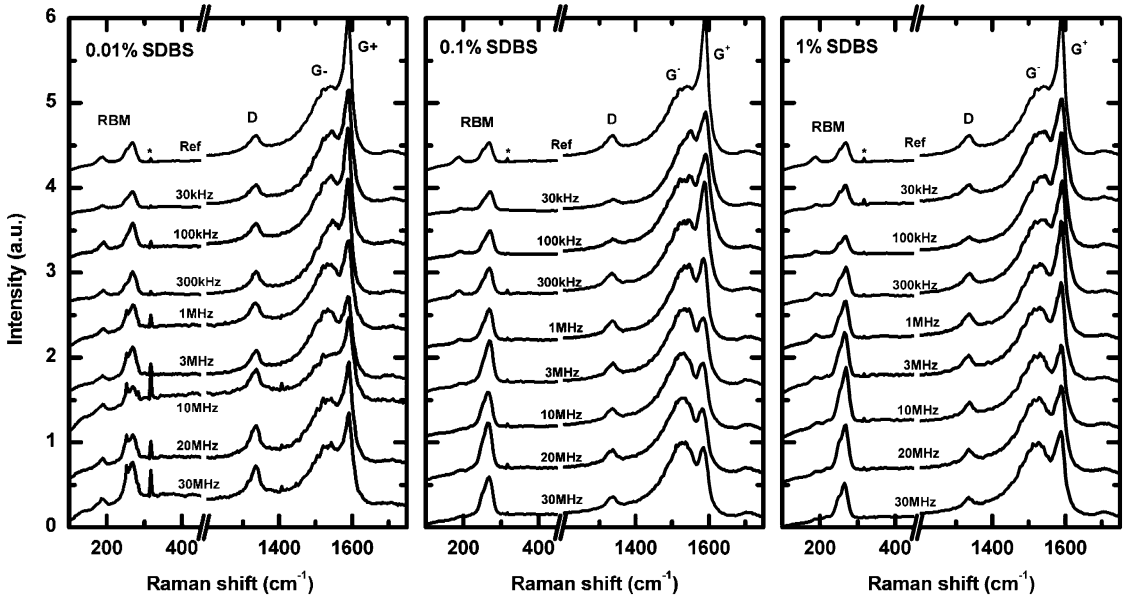

Figure 3. Raman spectroscopy on SWNTs deposited from (a) 0.01%, (b) 0.1%, and (c) 1% SDBS suspensions via dielectrophoresis at frequencies ranging from 30 kHz to 30 MHz and on reference samples. The probed semiconducting SWNTs contribute to radial breathing modes (RBM) around 180 cm^{-1} and to a sharp tangential (G^+) mode, the probed metallic SWNTs contribute to RBM modes around 260 cm^{-1} and to a broad G^- mode. Shown are the raw data including the disorder mode (D). Sharp spikes denoted as (*) are due to defective pixels of the detector. The spectra are normalized to the G^- mode and shifted vertically for clarity.

at any frequency. The result is not surprising since a prerequisite for successful separation are SWNTs being suspended individually (no bundle formation in suspension). However, in a 0.01% SDBS suspension with a soap concentration well below the CMC, heterogeneous bundles are already formed in suspension and inhibit a separation via DEP.

We now examine the 0.1% SDBS samples with individually suspended tubes (Figure 3b). Again we see for our reference sample contributions from both metallic and semiconducting SWNTs. For the samples prepared via DEP the spectra look different. At low-frequency we observe contributions of both metallic and semiconducting SWNTs. However, the Raman intensities are different compared to the reference sample. As we go from lower to higher frequencies, the G^+ mode becomes weaker (see also inset of Figure 6). Finally, above $f = 1$ MHz, the G^- mode becomes stronger than the G^+ mode and the RBM mode associated with semiconducting SWNTs vanishes. A similar, but somewhat less pronounced behavior is observed for the 1% SDBS samples,[7] with the content of semiconducting SWNTs being substantially reduced above $f = 3$ MHz (Figure 3c). Overall, the data demonstrate for the 0.1% and 1% SDBS samples the existence of a crossover frequency ω_c, where above only metallic SWNTs are deposited onto the microelectrode array, whereas below ω_c metallic and semiconducting SWNTs are deposited. Furthermore, ω_c shows a dependence on the conductivity of the surrounding liquid σ_l. This observation is summarized in Figure 4. We note that within our spectral resolution we do not observe significant shifts of the D mode around 1334 cm^{-1} or the G^+ mode around 1588 cm^{-1} mode for any of our samples. For the separated samples, we observe the expected downshift of the G- mode around 1524 cm^{-1} for metallic tubes[8]

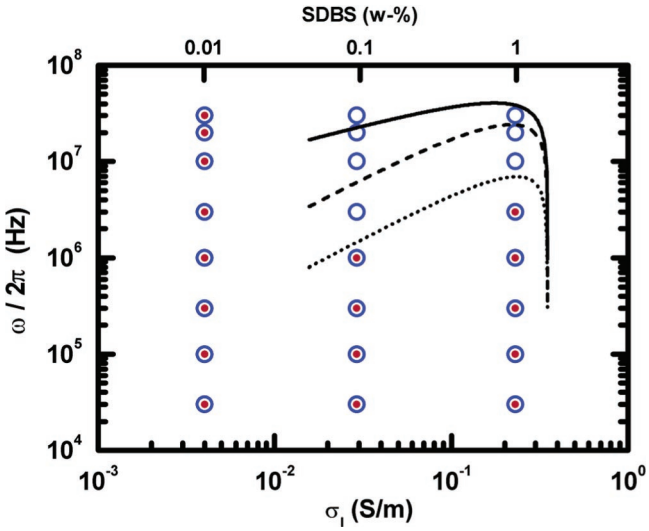

Figure 4. Dielectrophoretic deposition of metallic (○) and semiconducting (●) SWNTs as a function of frequency ω and suspension conductivity σ_l or surfactant concentration. For semiconducting SWNTs, a crossover frequency ω_c from positive DEP at $\omega < \omega_c$ to negative DEP at $\omega < \omega_c$ is observed. The full line shows the calculated ω_c for semiconducting SWNTs, with $\sigma_t = 0.35$ S/m following eq 1. The dotted and dashed lines depict the frequency where the attractive force $F_{DEP}(\omega)$ has dropped by 5% and 50% with respect to $F_{DEP}(0)$ upon approaching ω_c (see also Figure 6). Preformed bundles are present in the 0.01% SDBS suspension.

as compared to 1545 cm^{-1} for samples containing metallic and semiconducting tubes.

For a theoretical explanation of the observed frequency dependence we consider the DEP exerted on a tube of cylindrical shape and also take the ohmic losses of the tube and the suspension into account. Equation 1 describes the dielectrophoretic force derived for a long rod with its major

axis parallel to an inhomogeneous alternating electric field E of angular frequency ω.[9] ϵ_t^* and ϵ_l^* are the complex dielectric constants of the tube and the surrounding liquid. ϵ and σ are the corresponding dielectric constant and conductivity; d and l denote the diameter and length of a tube.

$$F_{\mathrm{DEP}} = \frac{\pi d^2 l}{8}\epsilon_l \mathrm{Re}\left(\frac{\epsilon_t^* - \epsilon_l^*}{\epsilon_l^* + (\epsilon_t^* - \epsilon_l^*)L}\right)\nabla E^2$$

$$\epsilon_{t,l}^* = \epsilon_{t,l} - i\frac{\sigma_{t,l}}{\omega} \qquad (1)$$

The depolarization factor L is of the order of 10^{-5} for HiPco tubes having a diameter between 0.8 and 1.4 nm and a length between 300 nm and 1 μm.[10] Concerning the dielectric properties of the solvent, we have used SDBS concentrations of 0.01%, 0.1%, and 1%, yielding σ_l equal to 4 mS/m, 29 mS/m, and 230 mS/m, respectively. ϵ_l varies between $75\epsilon_0$ and $85\epsilon_0$ depending on the surfactant concentration and on the frequency of the electric field.[11] To calculate the sign of the force we have to compare the dielectric properties of the suspension with the corresponding properties of the SWNTs.

Metallic SWNTs have a conductivity and a dielectric constant many orders of magnitude larger than those of water, even for high surfactant concentrations.[12] According to eq 1 metallic tubes undergo *positive* DEP ($F_{\mathrm{DEP}} > 0$) at any frequency and any soap concentration experimentally accessible, as observed in our experiment. For semiconducting SWNTs with ϵ_t between $2\epsilon_0$ and $5\epsilon_0$, depending on the tube diameter[12] and with a zero intrinsic conductivity, the DEP should be *negative* ($F_{\mathrm{DEP}} < 0$) at any frequency and soap concentration. However, a crossover from positive to negative DEP is observed for the 0.1% and 1% SDBS samples. This we can only explain by assigning a finite conductivity to the semiconducting SWNTs. We exclude a sizable conductivity of the tube itself induced by doping because the fluorescence signal of our suspensions (not shown here) is similar to nominally undoped SWNTs. Hence the origin of the conductivity must be due to a surface effect similar to earlier experiments with nanoparticles such as latex beads and the tobacco mosaic virus[13,14] where an electrical double layer at the solid−liquid interface modifies the dielectric properties of small particles. In our experiment, dodecylbenzene sulfonate molecules are adsorbed at the tube surface and we propose that the electrical double layer is formed by negatively charged benzene sulfonate headgroup ions and the sodium counterions. Sodium ions can be adsorbed at the headgroups, in the Stern layer, or form a diffusive layer. Both layers can contribute to a sizable surface conductance.[13] A qualitative fit to the observed frequency dependence is obtained with $\sigma_t = (0.35 \pm 0.1)$ S/m and $\epsilon_t = 5\epsilon_0$ [ϵ (dodecanol) $= 5.8\epsilon_0$] for the micellated tube, taking into account a substantial weakening of the positive DEP force already at $\omega \ll \omega_c$ as discussed below (Figure 6). Lacking the exact structure of the SDBS micelle formed around a SWNT, we cannot derive the conductivity from a microscopic model at the moment. However, our data compare

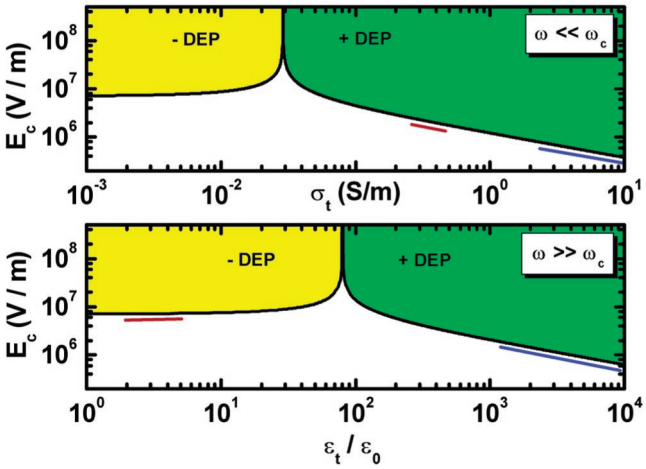

Figure 5. Minimum electric field strength E_c required to move a micellated SWNT (5 nm diameter and 500 nm length) via dielectrophoresis in a 0.1% SDBS suspension. In the low-frequency limit (top panel), E_c depends on the conductivity σ_t of the micellated tube. In the high-frequency limit (bottom panel), E_c depends on the dielectric constant ϵ_t. Values for E_c, corresponding to this experiment, are underlined for metallic (blue) and semiconducting (red) SWNTs. For $E > E_c$, the regions with observable positive dielectrophoresis (green) and negative dielectrophoresis (yellow) are marked.

well with DEP experiments with the rod-shaped tobacco mosaic virus (TMV) in a potassium phosphate buffer, yielding a surface-induced conductivity of $\sigma = 0.085$ S/m.[14] Note that the TMV has a diameter 10 times larger than that of SWNTs.

Now we study in more detail the DEP forces on metallic and semiconducting SWNTs and the consequences for the composition of samples deposited at low frequency. First we calculate the minimum field strength E_c needed for manipulating tubes via DEP. Because of the size of a tube, we assume that the major competing force comes from Brownian motion and we neglect electrohydrodynamical forces. We estimate E_c by setting the DEP potential energy equal to the thermal energy[15] kT with $T = 300$ K and $L = 0$. Equation 2 describes the high ($\omega \gg \omega_c$) and low ($\omega \ll \omega_c$) frequency limits of E_c, depending on whether the real part or the imaginary part of ϵ^* are dominating the DEP:

$$E_c(\omega \gg \omega_c) \simeq \sqrt{\frac{kT}{\frac{\pi d^2 l}{8}\epsilon_l \mathrm{Re}\left(\frac{|\epsilon_t - \epsilon_l|}{\epsilon_l}\right)}}$$

$$E_c(\omega \ll \omega_c) \simeq \sqrt{\frac{kT}{\frac{\pi d^2 l}{8}\epsilon_l \mathrm{Re}\left(\frac{|\sigma_t - \sigma_l|}{\sigma_l}\right)}} \qquad (2)$$

E_c is plotted in Figure 5 for the micellated tube with $d = 5$ nm and $l = 500$ nm in a 0.1% SDBS supension.[16] For our experiment, with the dielectric properties of both tube types and of the solvent being significantly different from each other, we see that the minimum electric field strength is on the order of 10^6 V/m, which is in agreement with our experimental observation. Concerning the low-frequency

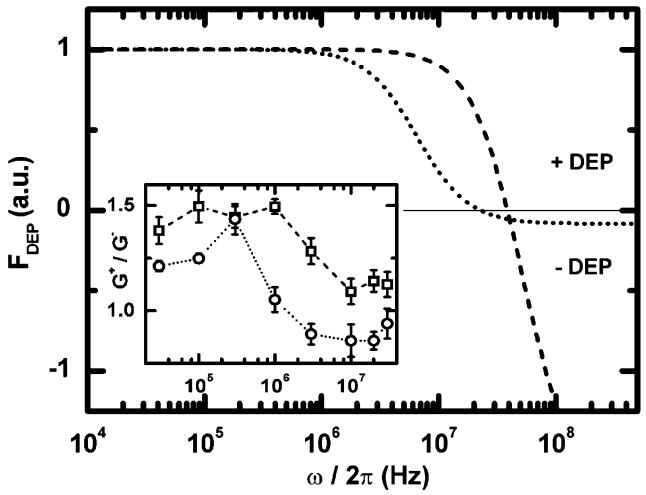

Figure 6. Calculated dielectrophoretic force F_{DEP} on a semiconducting SWNT in a 0.1% SDBS suspension (dotted line) and a 1% SDBS suspension (dashed line) with $\sigma_t = 0.35$ S/m. Inset shows the ratio of the G^+ mode to the G^- mode for deposits from corresponding suspensions (circle = 0.1% SDBS; square = 1% SDBS) with lines as guide to the eye. The experiment probes the initial decrease of F_{DEP} due to experimental limitation of E close to E_c (see Figure 5).

range of our experiments, where positive DEP is observed for both tube types, we see that E_c is smaller for better conducting tubes. Hence positive DEP forces are stronger for metallic than for semiconducting SWNTs, giving rise to a different and field-dependent composition of the low-frequency DEP samples from 0.1% and 1% SDBS suspensions, as compared to the reference sample. This effect is not observed for the 0.01% SDBS sample with preformed bundles, as expected.

The results support the general concept of surface-induced conductivity, even for micelle suspended single-walled carbon nanotubes. In particular, the data demonstrate that dielectrophoresis at high electric field frequency allows to separate metallic from semiconducting SWNTs owing to the different sign of the dielectrophoretic force for each tube type. At low frequency, dielectrophoresis can be used for a site-selective deposition of both tube types, e.g., from separated fractions. Moreover, dielectrophoresis should allow to further fractionate according to length and diameter since E_c is proportional to d^{-1} and to $l^{-1/2}$. Finally, knowing the electromechanical response of individually suspended SWNTs enables to understand the response of SWNT bundles or of multiwalled carbon nanotubes, which contain metallic and semiconducting tubes.[17−21]

Acknowledgment. The authors acknowledge M. P. Hughes for valuable information, R. Smalley for providing raw soot of HiPco SWNTs, and D. Beckmann, D. Secker, and H. B. Weber for helpful discussions.

References

(1) Saito, R.; Dresselhaus, G.; Dresselhaus, M. S. *Physical properties of carbon nanotubes*; Imperial College Press: London, 1998.
(2) Li, Y.; Mann, D.; Rolandi, M.; Kim, W.; Ural, A.; Hung, S.; Javey, A.; Cao, J.; Wang, D.; Yenilmez, E.; Wang, Q.; Gibbons, J. F.; Nishi, Y.; Dai, H. *Nano Lett.* **2004**, *4*, 317−321.
(3) Krupke, R.; Hennrich, F.; v. Löhneysen, H.; Kappes, M. M. *Science* **2003**, *301*, 344−347.
(4) O'Connell, M. J.; Bachilo, S. M.; Huffmann, C. B.; Moore, V. C.; Strano, M. S.; Haroz, E. H.; Railon, K. L.; Boul, P. J.; Noon, W. H.; Kittrell, C.; Ma, J.; Hauge, R. H.; Weisman, R. B.; Smalley, R. E. *Science* **2002**, *297*, 593−596.
(5) Hait, S. K.; Majhi, P. R.; Blume, A.; Moulik, S. P. *J. Phys. Chem. B* **2003**, *107*, 3650−3658.
(6) Heller, D. A.; Barone, P. W.; Swanson, J. P.; Mayrhofer, R. M.; Strano, M. S. *J. Phys. Chem. B* **2004**, *108*, 6905−6909.
(7) In 1% SDBS suspensions, we observe that micelles tend to agglomerate with time, lowering the separation yield.
(8) Dresselhaus, M. S.; Dresselhaus, G.; Jorio, A.; Souza Filho, A. G.; Saito, R. *Carbon* **2002**, *40*, 2043−2061.
(9) Jones, T. B. *Electromechanics of particles*; Cambridge University Press: Cambridge, 1995.
(10) For a needle-shaped particle aligned with the electric field lines, the depolarization factor L can be approximated by $L = d^2/l^2$ [ln($2l/d$) − 1]. See ref 9.
(11) Pérez-Rodríguez, M.; Varela, L. M.; García, M.; Mosquera, V.; Sarmiento, S. *J. Chem. Eng. Data* **1999**, *44*, 944−947.
(12) Benedict, L. X.; Louie, S. G.; Cohen, M. L. *Phys. Rev. B* **1995**, *52*, 8541−8549.
(13) Hughes M. P. *J. Colloid Interface Sci.* **2002**, *250*, 291−294. We neglect here also dielectric losses at the tube/liquid interface.
(14) Morgan, H.; Green, N. G. *J. Electrostatics* **1997**, *42*, 279−293.
(15) Ramos, A.; Morgan, H.; Green, N. G.; Castellanos, A. *J. Phys. D: Appl. Phys.* **1998**, *31*, 2338−2353.
(16) For the diameter of the object tube+micelle we refer to a molecular dynamic simulation of tube+SDS in ref 4.
(17) Yamamoto, K.; Akita, S.; Nakayama, Y. *J. Phys. D: Appl. Phys.* **1998**, *31*, L34−L36.
(18) Chen, X. Q.; Saito, T.; Yamada, H.; Matsushige, K. *Appl. Phys. Lett.* **2001**, *78*, 3714−3716.
(19) Nagahara, L. A.; Amlani, I.; Lewenstein, J.; Tsui, R. K. *Appl. Phys. Lett.* **2002**, *80*, 3826−3828.
(20) Krupke, R.; Hennrich, F.; Weber, H. B.; Beckmann, D.; Hampe, O.; Malik, S.; Kappes, M. M.; v. Löhneysen, H. *Appl. Phys. A* **2003**, *76*, 397−400.
(21) Suehiro, J.; Zhou, G.; Hara, M. *J. Phys. D: Appl. Phys.* **2003**, *36*, L109−L114.
(22) Krupke, R.; Hennrich, F.; Weber, H. B.; Kappes, M. M.; v. Löhneysen, H. *Nano Lett.* **2003**, *3*, 1019−1023.

NL0493794